

Full Length Research Paper

Influence of Indian Ocean zonal circulation on variability and predictability of Ethiopia highlands vegetation

Mark R. JuryUniversity Puerto Rico Mayaguez, PR 00681, USA.
University Zululand, KwaDlangezwa 3886, South Africa.

Received 26 May, 2015; Accepted 10 September, 2015

The vegetation fraction over the Ethiopian highlands exhibits large seasonal and multi-annual variability in the period 1982 to 2014. Northern areas are more sensitive to rainfall due to the brevity of the wet season. Differences in the regional climate during periods of high and low vegetation are analyzed using composite fields of rainfall, wind, humidity, sea temperatures, salinity and currents; and correlations at six-month lead-time. The key climatic driver of vegetation is the zonal overturning atmospheric circulation linking subsidence over the east Indian Ocean and ascent within an expanded African monsoon. Certain aspects of this Walker Cell reflect Pacific ENSO interaction with the Indian Ocean Dipole. During cold phase ENSO an upwelling Rossby wave and cool sea temperatures in the west Indian Ocean promote vegetation growth in the Ethiopian highlands.

Key words: Vegetation, climate forcing, prediction, Ethiopia.

INTRODUCTION

Semi arid parts of Africa bordering the Congo monsoon, such as the Sahel and Zambezi, are characterised by high rainfall variability and low yield agriculture that contribute to food insecurity (Cassel-Gintz et al., 1997). To better understand how summer rainfall affects crop production at state-level, past work has compared time series of farm yields, rain-gauge and satellite data (Tucker, 1979; Eklundh, 1998; Richard and Pocard, 1998; Al-Bakri and Suleiman, 2004; Budde et al., 2004). Remotely sensed color reflectance is used to quantify vegetation fraction since 1982 (Bannari et al., 1995), with bias correction for sensor degradation, orbital drift and

atmospheric contamination (Chappell et al., 2001; Kawabata et al., 2001; Mennis, 2001; Tucker et al., 2005), and intercomparisons with crop yield (Lewis et al., 1998; Maselli et al., 2000). Rainfall in semi-arid zones drives vegetation growth at seasonal and multi-annual time scales (Budde et al., 2004; Eklundh and Sjöström, 2005; Li et al., 2004; Vanacker et al., 2005) with a response lag of one to two months (Davenport et al., 1993; Eklundh, 1998; Richard and Pocard, 1998). Correlations between vegetation fraction and rainfall are higher for running sums and in zones with a single wet season of 600 to 1000 mm (Davenport et al., 1993; Reed

*Corresponding author. E-mail: mark.jury@upr.edu

Author(s) agree that this article remain permanently open access under the terms of the [Creative Commons Attribution License 4.0 International License](https://creativecommons.org/licenses/by/4.0/)

et al., 1994; White, 1997; Herrmann et al., 2005; Vanacker et al., 2005; Zhang et al., 2005); whereas vegetation sensitivity to climate in desert and monsoon regions is limited.

Previous research has shown that the El Niño/Southern Oscillation (ENSO) modulates vegetation across Africa (Ropelewski and Halpert, 1987; Myneni et al., 1996; Kogan, 1998; Verdin et al., 1999; Plisnier et al., 2000; Mennis, 2001; Anyamba et al., 2002). Changes in tropical Pacific Ocean sea surface temperatures (SST) influence the overlying atmospheric convection and zonal circulation, with effects spreading globally across the Atlantic and Indian Oceans. Interaction between winds in the western Pacific and SST in the Indian Ocean can modulate ENSO onset or decay (Annamalai et al., 2005; Kug et al., 2005, 2006). In addition to the basin-wide signal forced by ENSO through the Walker circulation, air–sea coupling across the Indian Ocean generates a dipole mode (Saji et al., 1999), with opposing sea temperature anomalies linked by changes in the ocean circulation and Rossby wave activity (Annamalai et al., 2005).

When there is cold water upwelling in the eastern Pacific, the zonal atmospheric circulation generates rising motion over the western Pacific and Africa, every 3 to 7 years (Carleton, 1998; Young and Harris, 2005). Africa's vegetation responds to summer rainfall anomalies forced by ENSO (Ropelewski and Halpert, 1987); being more favourable to crop production during cold phase (Cane et al., 1994; Myneni et al., 1996; Mennis, 2001; Anyamba et al., 2002). Correlations between area-averaged vegetation and global SST have revealed ENSO signals, particularly for southern Africa where the summer rainfall coincides with mature ENSO phase (Anyamba and Eastman, 1996; Myneni et al., 1996; Kogan, 1998; Richard and Pocard, 1998; Anyamba et al., 2001). However links with North Africa are somewhat obscure and unpredictable, as the wet season (June–September) precedes ENSO maturity.

The main goals here are to understand the controls on late summer vegetation in Ethiopia's crop growing region and its links with global climate.

DATAS AND METHODS

The analysis scheme used to uncover the climatic drivers of Ethiopian vegetation is described. Our basis is the bias-corrected July to October satellite vegetation fraction (NDVI) from 1982 to 2014 (Huete et al., 2002; Tucker et al., 2005; Philippon et al., 2014) averaged over the Ethiopian highlands (box in Figure 1a). Atmosphere and ocean reanalysis fields are studied for patterns both simultaneously and in precursor season.

The target area is defined by crop production areas known to the Ethiopian Institute for Agricultural Research and the US Department of Agriculture, encompassing a zone 7–14N, 36.5 to 40.5E (Figure 1a) where vegetation fraction reaches 0.4 following the annual cycle of rainfall (Figure 1b and c). The Jun–Sep rainfall correlation

with July to October vegetation is highest in the northern sector (Tigray), where the uni-modal wet season is short (Figure 1d). Temporal lag correlations are greatest from 0 to 3 months (Figure 1e); while correlations with temperature are negative (not shown). Hence the northern highlands are more vulnerable to fluctuations of climate, and the focus of this study. The southern highlands have a bi-modal rainy season and vegetation fraction tends to be steadier and less sensitive to rainfall.

Vegetation fraction may be considered a proxy for Ethiopian crop yield, based on earlier validations (Jury, 2013). Drivers of the in-season (Jul–Oct) climate are studied by composite analysis of high vegetation minus low vegetation years: 1986, 1988, 1994, 1999, 2001, 2002 minus 1983, 1991, 1993, 1998, 2010, 2013. The difference field of GPCP rainfall (Adler et al., 2003) reflects a dipole between Africa and the Indian Ocean, so the area of composite analysis is 20S to 30N, 0 to 120E for maps, and 10S to 20N and 10 to 90E for vertical sections. Parameters include NCEP2 atmosphere reanalysis (Kanamitsu et al., 2002) humidity and zonal circulation, and NOAA ocean reanalysis (Behringer et al., 2007) temperature, salinity and zonal circulation. The composite methods are similar to Hastenrath (2000). A hovmoller analysis of 6-month running mean NOAA satellite outgoing longwave radiation (OLR) anomalies is made in the 10S to 20N latitude band 1982 to 2014, to investigate zonal propagation and dipole features. A useful attribute of OLR is its ability to reveal both convective (-) and subsident (+) weather.

Forecasts in April would be most useful for agricultural planning, so statistical predictors are drawn from the preceding December to March (winter) season. The July to October vegetation fraction is employed to 'find' predictors in global fields by correlation of December to March sea surface temperature (SST) from the Hadley Centre (Kennedy et al., 2011), and sea level pressure (SLP) and 850 hPa winds from the European Community Medium-range Weather Forecast (ECMWF) reanalysis (Dee et al., 2011). All time series are standardized and linearly detrended. Field correlations < 0.28 are deemed insignificant at 90% confidence and shaded neutral in this analysis Table 1.

Predictors were assembled from the 4 to 7 month lead-time correlation maps. The candidate predictor pool was eight over a training period of 32 years: 1982 to 2014. A statistical algorithm was formulated in MS Excel via backward stepwise linear regression onto the target time series. Initially all predictors were included and their partial correlation was evaluated. Those with lower significance (or co-linearity) were screened out and the algorithm was re-calculated with the remaining variables. Its performance was evaluated by r^2 fit, adjusted for the number of predictors. The time series have minimal persistence; statistical significance is achieved with r^2 fit > 0.42 with 31 degrees of freedom. Predicted vs observed scatterplots were analyzed for slope, tercile hits and outliers.

RESULTS

Drivers of in-season vegetation

The GPCP rainfall composite difference map for high minus low vegetation (Figure 2a) reflects a dipole between increased convective rainfall across Africa and dry weather over the east Indian Ocean, consistent with earlier work (Saji et al., 1999; Jury and Huang, 2004; Luo et al., 2010). The African monsoon that is most intense over the Congo basin, tends to expand. Hovmoller analysis of satellite OLR anomalies in latitudes of Ethiopia (Figure 2b) exhibit weak or eastward propagation

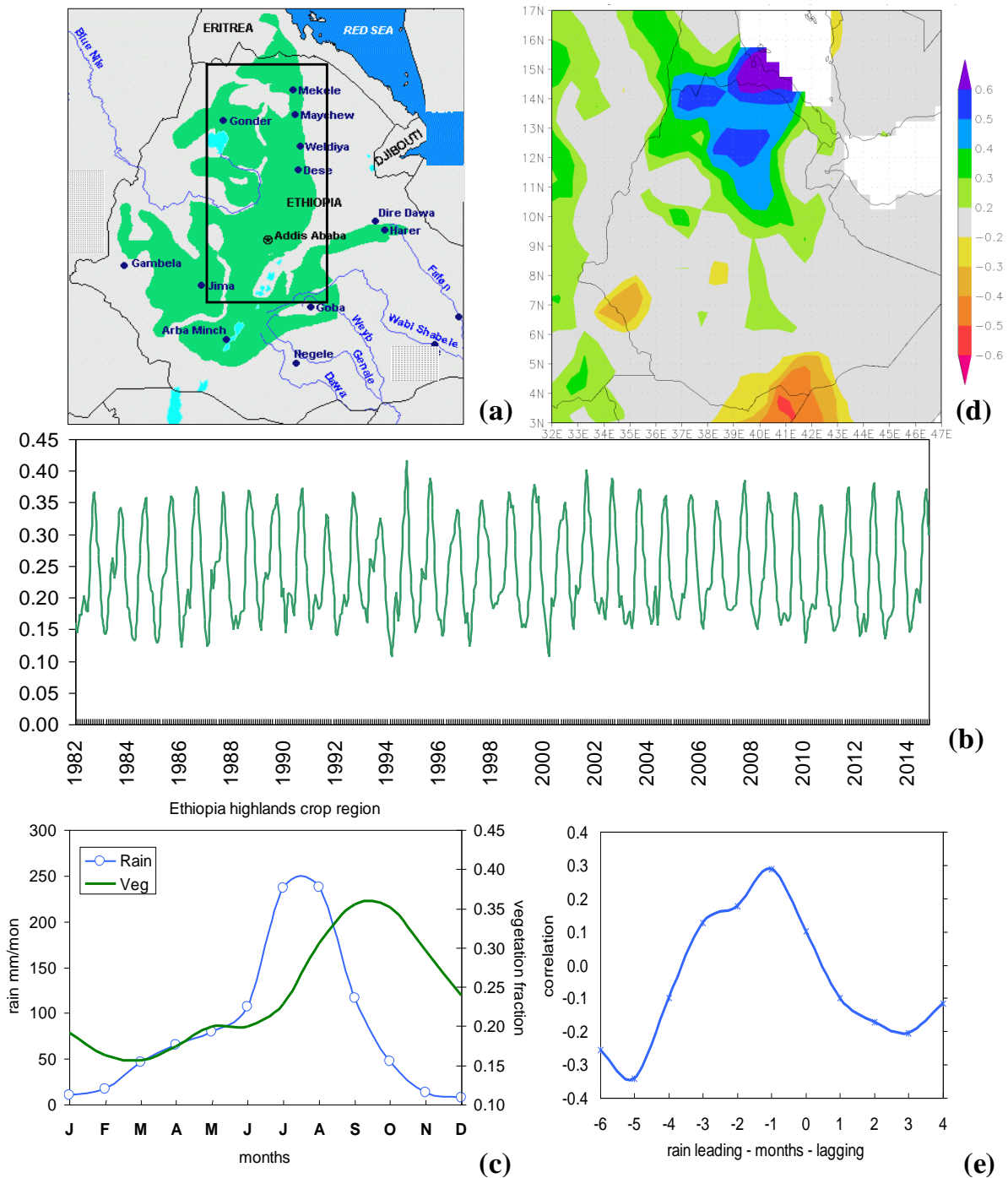


Figure 1. (a) Crop production area of the Ethiopian highlands and target area (box), (b) time series of vegetation index, (c) mean annual cycle of rainfall and vegetation fraction in the target area, (d) correlation map of Jun-Sep rainfall with Jul-Oct vegetation, (e) temporal correlation of local rainfall at various leads and lags and July-Oct vegetation. July to October vegetation is plotted in Figure 6a.

of sustained convective features; dipole conditions are seen over the Indian Ocean less than half the time.

The height section of composite high minus low

humidity and zonal circulation reflects a dry zone southeast of India where subsidence is found (Figure 3a and b), and a wet zone over Africa where uplift is evident.

Table 1. Datasets used in the statistical analysis. References are listed in text, web sources are given in acknowledgement.

	Name	Resolution (km)
ECMWF	European Centre for Medium-Range Weather Forecasts (interim) Reanalysis	80
GPCP2	Global Precipitation Climatology Project v2 satellite-gauge rainfall	200
NCEP2	National Centers for Environmental Prediction v2 Reanalysis	180
NDVI	Normalized Difference Vegetation Index (NASA)(bias-corrected)	30
NOAA	Global Ocean Data Assimilation System (Reanalysis)	70
OLR	Outgoing Long-wave Radiation from NOAA satellite (bias-corrected)	200 km
SST	Hadley Centre satellite-ship Reanalysis of sea surface temperature	100 km

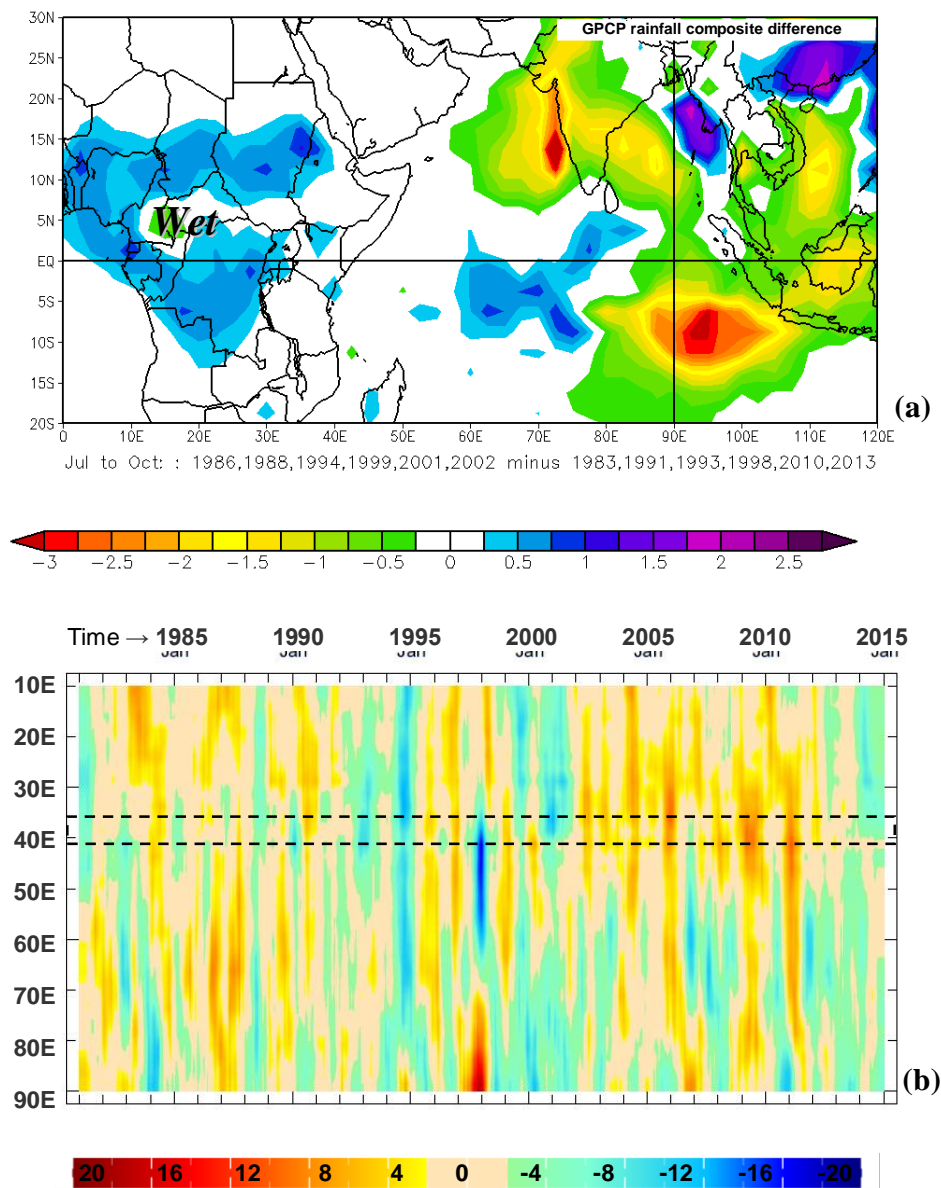


Figure 2. (a) Composite high minus low (vegetation) difference of Jul-Oct GPCP satellite rainfall (mm/day). (b) Hovmoller analysis of satellite OLR anomalies (W/m^2) averaged 10S-20N, with dashed area of Ethiopia.

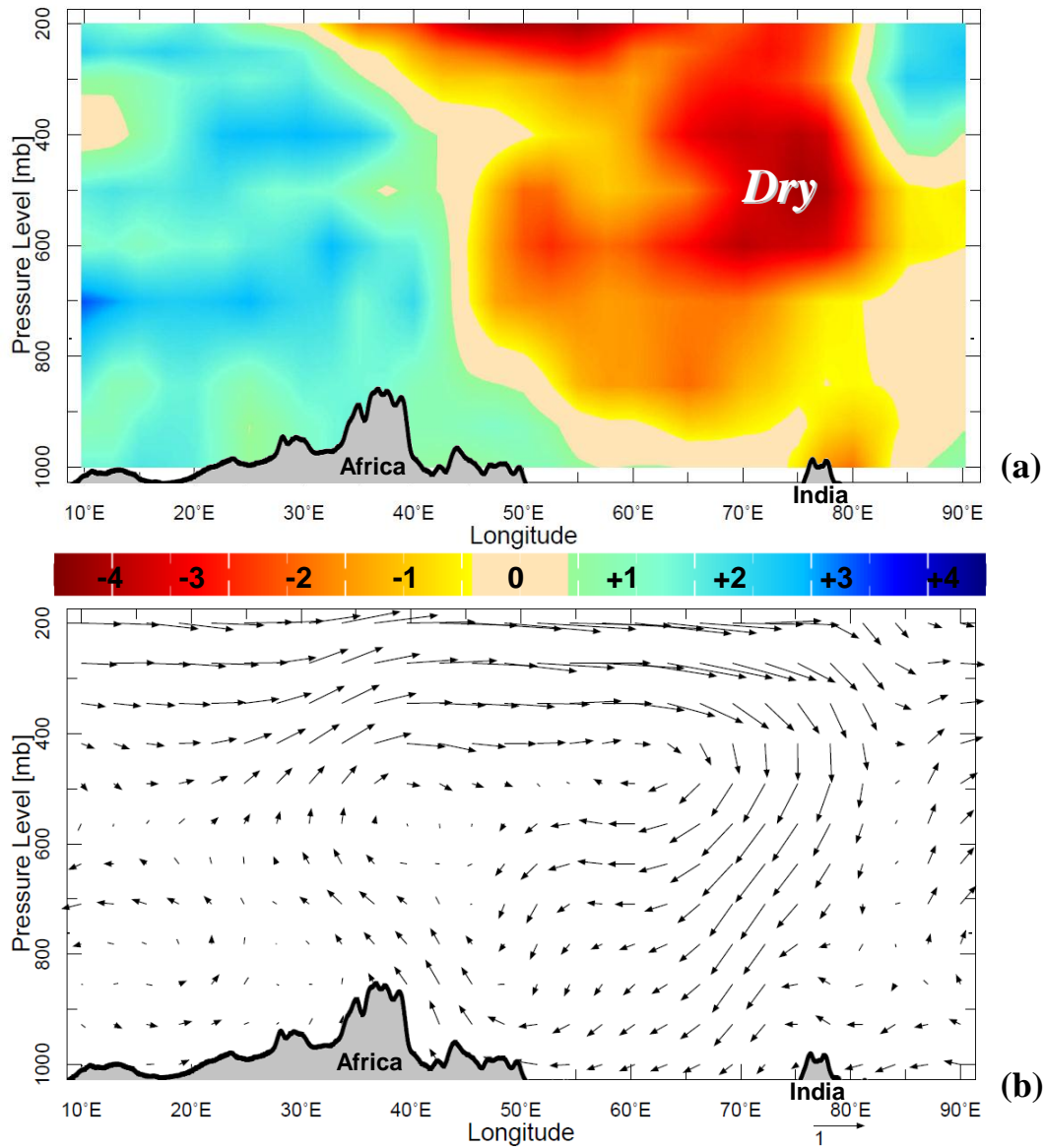


Figure 3. Composite high minus low (vegetation) difference of July to October atmospheric (a) relative humidity (%) and (b) zonal circulation (m/s), in height section averaged 10S-20N with topography.

Surface easterly / upper westerly wind differences complete the zonal overturning atmospheric circulation. The upper ocean composite difference patterns (Figure 4a to c) show a cool anomaly in 40-100 m depths 40 to 65E, and a warm anomaly 60 to 120 m 75-90E, a pattern consistent with Indian Ocean Dipole during Pacific La Niña. The zonal ocean circulation differences reflect westward flow at depth that upwells at 50E. Above the warm zone in the east Indian Ocean near-surface current differences are also westward, but near Africa they are eastward and thus convergent in the central basin. Fresh waters are noted off Africa that correspond with surplus

rainfall and run-off, but extend to depths of 300 m.

Elsewhere in the east Indian Ocean, salinity differences are positive above 60m, consistent with evaporation exceeding precipitation there.

Lag correlation and prediction

The July to October vegetation values (1982-2014) are correlated with global fields in December to March season to generate predictor maps (Figure 5a to c). SST fields in respect of vegetation exhibit a cooler west Indian

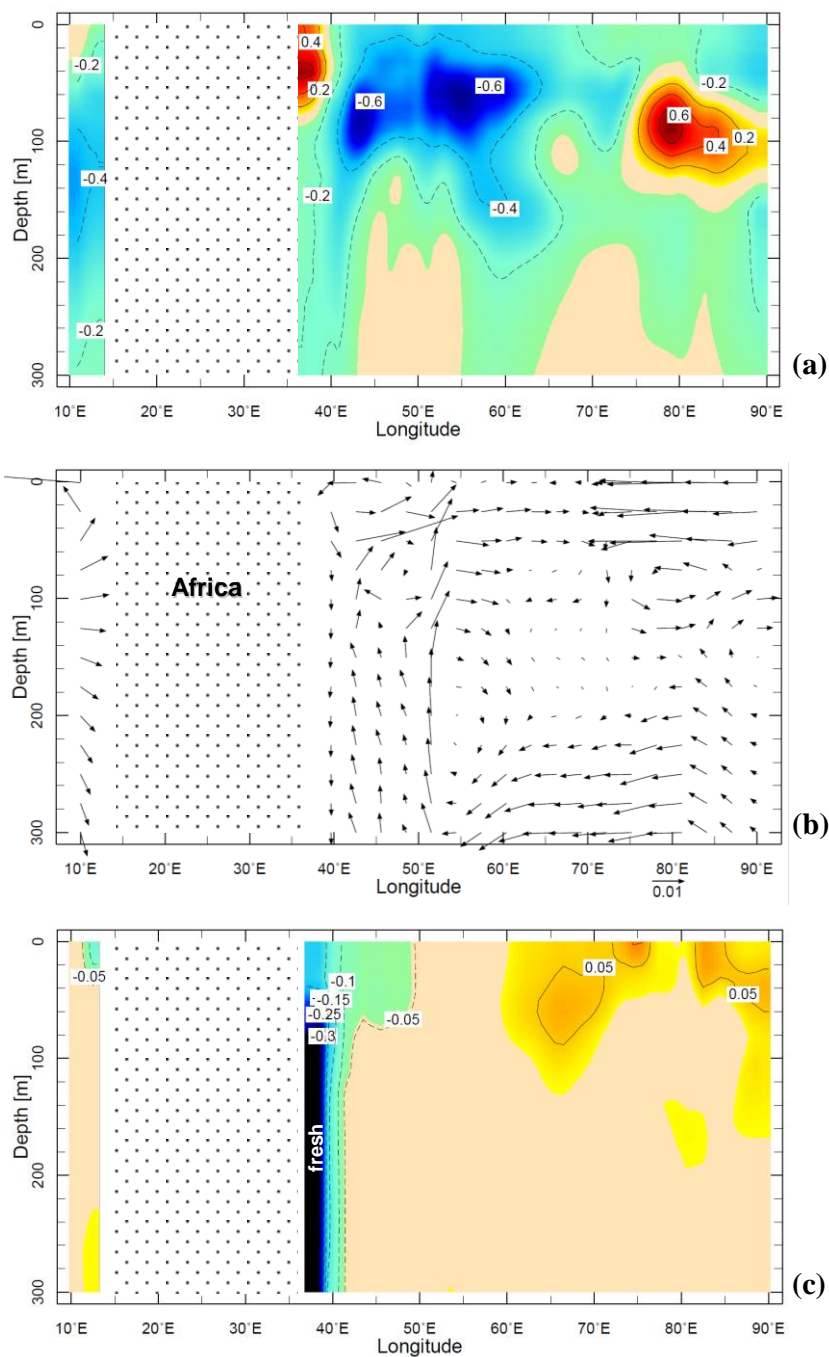


Figure 4. Composite high minus low (vegetation) difference of Jul-Oct subsurface ocean (a) temperature, (b) zonal circulation and (c) salinity (ppt), in depth section averaged 10S-20N.

Ocean and warmer west Pacific Ocean similar to Rowell (2013), but elsewhere weak values are found. The ENSO (cold) signal is ‘not ready’ in the preceding year. The December to March sea level air pressure map is dominated by a global dipole of positive values over the

Americas and negative values over Southeast Asia. This wave-one feature is consistent with the decadal dipole of White and Tourre (2003, 2007) that refers to an interaction of ENSO and south Indian Ocean Rossby wave (Jury and Huang, 2004). As a result of the high

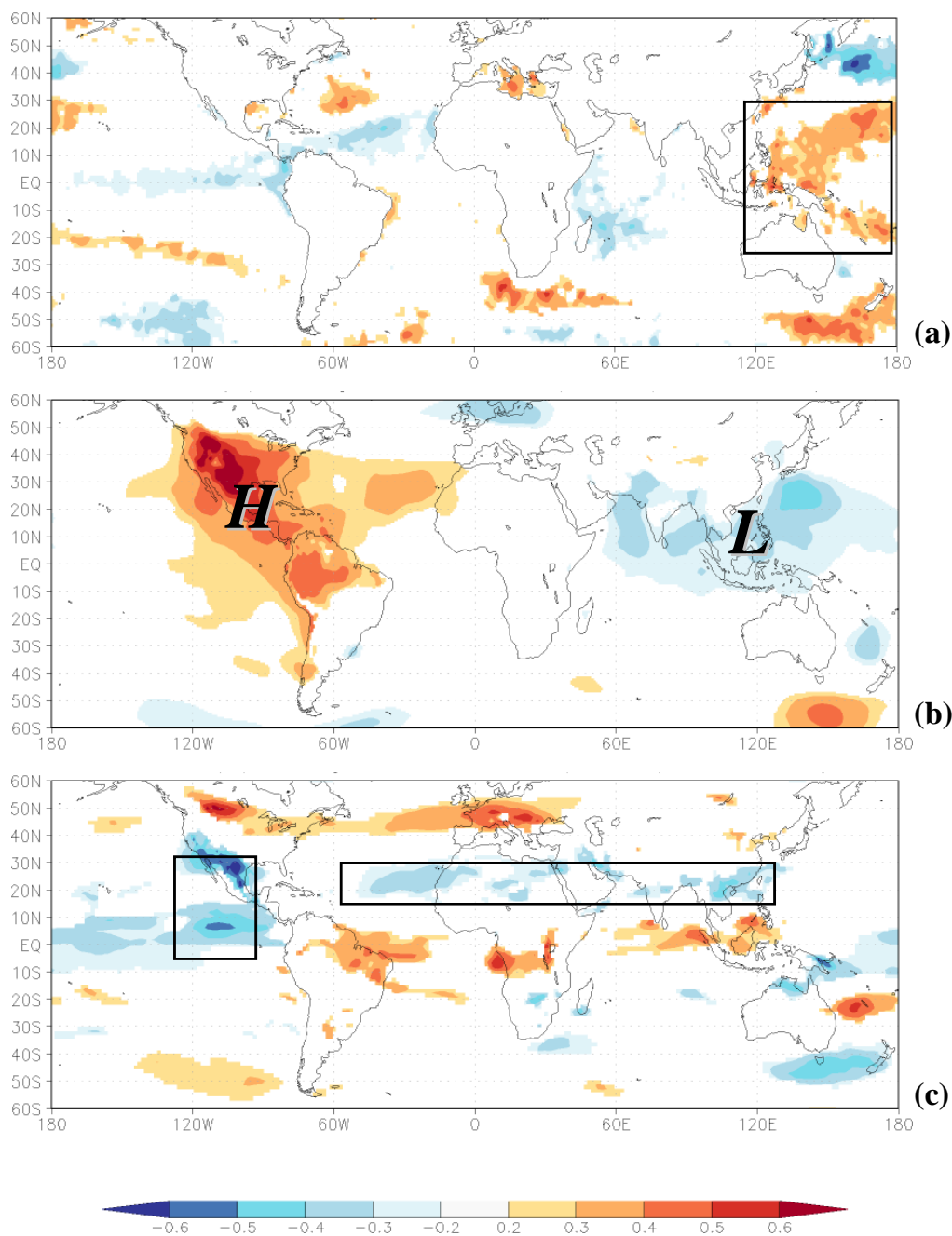


Figure 5. Correlation maps at December to March lead time in respect of July to October vegetation for (a) SST, (b) SLP, and (c) 850 hPa zonal wind. Predictors used in the multi-variate algorithm are identified with boxes. Insignificant correlations are shaded neutral.

pressure over the Americas, the zonal wind correlations are negative over the northeast Pacific. Elsewhere there is a band of negative correlation across North Africa and Southern China and an opposing band of positive zonal wind correlation near the equator from Brazil to the Maritime Continent. A positive correlation also exists across the north Atlantic mid-latitudes. These patterns for

the preceding December to March are useful to extract key predictor time series and develop a multi-variate algorithm to forecast changes in July to October vegetation fraction, as a proxy for crop yield in Ethiopia. After back-ward stepwise regression and elimination of weaker predictors, a three parameter algorithm is formed that generates a 6-month lead forecast. The time series

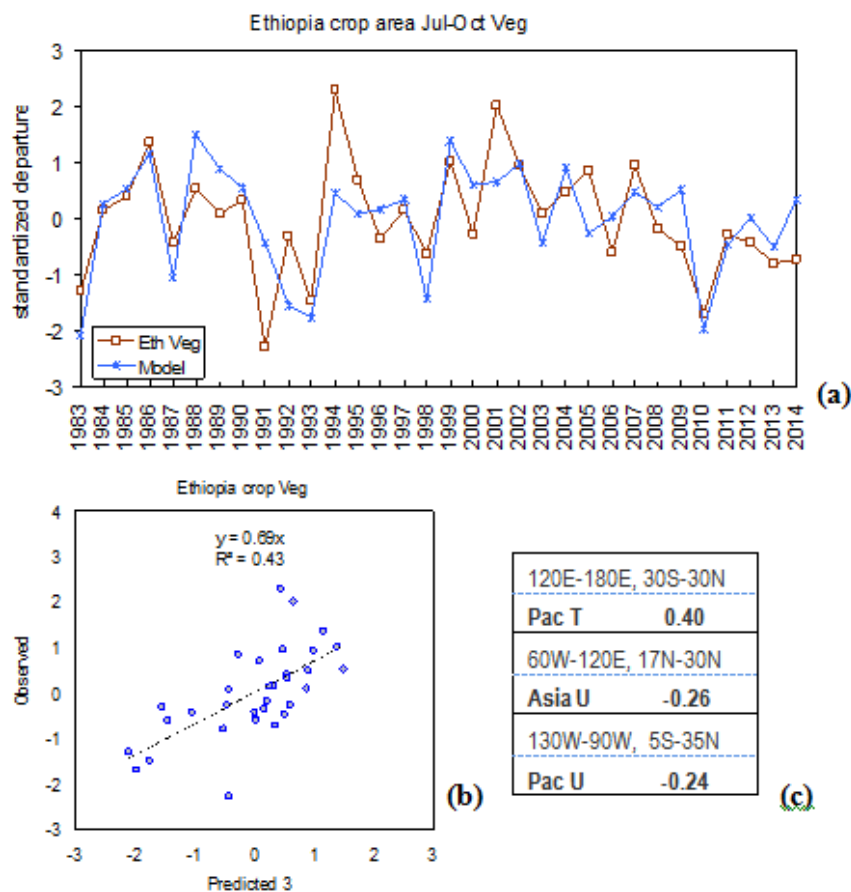


Figure 6. Observed and predicted Ethiopian highlands July to October vegetation as (a) time series and (b) scatterplot and fit. (c) Table of predictor domain and influence (bold).

and scatterplot comparisons are given in Figure 6a and b. The leading predictor is west Pacific SST (warm favourable), followed by Asia zonal winds and Pacific zonal winds (easterly favourable). The model fit (43%) is on the borderline of statistical significance, typical for northern summer climate. The tercile hit rate is 64% in the below category, with misses in 1991 and 2014, and 82% in the above category, with misses in 1995 and 2005. The model predicts low vegetation fraction in 1983, 1993 and 2010, but under-predicts the high years of 1994 and 2001. The predictors apparently foretell of chances for a convective dipole between the east Indian Ocean and central Africa (Figure 2a).

Conclusions

The vegetation fraction over the Ethiopian highlands exhibits large seasonal and multi-annual variability in the period 1982 to 2014. Northern areas are more sensitive to rainfall due to the brevity of the wet season and

proximity to arid zones. In comparison with parallel work using rainfall over the same place and era, our vegetation index exhibits markedly different teleconnections.

The regional climate influence was expressed in (high minus low vegetation) composites of rainfall, wind, humidity, sea temperatures, salinity and currents; and correlations at six-month lead-time. The key climatic driver of vegetation is the zonal overturning atmospheric circulation linking subsidence over the east Indian Ocean and ascent within an expanded African monsoon (Figure 3a and b). Certain features of this Walker Cell reflect Pacific ENSO interaction with the Indian Ocean Dipole (Figure 4a) which, during cold phase, induces an upwelling Rossby wave and cool sea temperatures, as outlined in White and Tourre (2007). It is odd that convection is suppressed over India during years of above normal vegetation in Ethiopia, as prior work has shown that an active Indian monsoon enhances the upper easterly jet and Nile River flow (Camberlin, 1997; Jury, 2011). Further study of this feature and its stability is needed.

Conflict of Interest

The authors have not declared any conflict of interest.

ACKNOWLEDGEMENTS

This study is part of a Rockefeller Foundation project with the Ethiopian Institute for Agricultural Research, Melkasa, conceived with help from F. Mequanint and G. Mamo. Web-based analyses were made using the IRI Climate Library, the KNMI Climate Explorer, and the NCEP ESRL-PSD composite mapping system.

REFERENCES

- Adler RF, Huffman GJ, Chang A, Ferraro R, Ping-Ping X, John J, Bruno R, Udo S, Scott C, David B, Arnold G, Joel S, Philip A, Eric N (2003). The version 2 Global Precipitation Climatology Project (GPCP) monthly precipitation analysis (1979-Present). *J. Hydrometeorol* 4:1147-1167.
- Al-Bakri JT, Suleiman AS (2004). NDVI response to rainfall in different ecological zones in Jordan. *Int. J. Remote Sens.* 25:3897-3912.
- Annamalai H, Xie S-P, McCreary JP, Murtugudde R (2005). Impact of Indian Ocean sea surface temperature on developing El Niño. *J. Clim.* 18:302-319.
- Anyamba A, Eastman JR (1996). Interannual variability of NDVI over Africa and its relation to El Niño/Southern Oscillation. *Int. J. Remote Sensing* 17:2533-2548.
- Anyamba A, Tucker CJ, Eastman JR (2001). NDVI anomaly patterns over Africa during the 1997/98 ENSO warm event. *Int. J. Remote Sensing* 22:1847-1859.
- Anyamba A, Tucker CJ, Mahoney R (2002). From El Niño to La Niña: Vegetation response patterns over eastern and southern Africa during the 1997-1998 period. *J. Clim.* 15:3096-3103.
- Bannari A, Morin D, Bonn F (1995). A review of vegetation indices. *Remote Sensing Rev.* 13:95-120
- Behringer DW (2007). The Global Ocean Data Assimilation System (GODAS) at NCEP. Proc. 11th Symp. Integr. Obs. Assim. Systems, San Antonio, TX, Amer. Meteor. Soc. 3.3.
- Budde ME, Tappan G, Rowland J, Lewis J, Tieszen LL (2004). Assessing land cover performance in Senegal, West Africa using 1-km integrated NDVI and local variance analysis. *J. Arid Environ.* 59:481-498.
- Cane MA, Eshel G, Buckland RW (1994). Forecasting Zimbabwean maize yield using eastern equatorial Pacific sea-surface temperature. *Nature* 370:204-205.
- Camberlin P (1997). Rainfall anomalies in the source region of the Nile and their connection with the Indian summer monsoon. *J. Clim.* 10:1380-1392.
- Carleton AM (1998). Ocean-Atmosphere Interactions, in Encyclopedia of Environmental Analysis and Remediation. RA Meyers (ed), Wiley, New York. Pp. 3151-3188.
- Cassel-Gintz MA, Lüdeke MKB, Petschel-Held G, Reusswig F, Pöchl M, Lammell G, Schellnhuber HJ (1997). Fuzzy logic based global assessment of marginality of agricultural land use. *Clim. Res. Int. Clim. Ecosys. Human Soc.* 8:135-150.
- Chappell A, Seaquist JW, Eklundh L (2001). Improving the estimation of noise from NOAA AVHRR NDVI for Africa using geostatistics. *Int. J. Remote Sensing* 22:1067-1080.
- Davenport ML, Nicholson SE (1993). On the relation between rainfall and the Normalized Difference Vegetation Index for diverse vegetation types in East Africa. *Int. J. Remote Sens.* 14:2369-2389.
- Dee DP, Uppala SM, Simmons AJ, Berrisford P, Poli P, Kobayashi S, Andrae U, Balmaseda MA, Balsamo G, Bauer P, Bechtold P, Beljaars ACM, van de Berg L, Bidlot J, Bormann N, Delsol C, Dragani R, Fuentes M, Geer AJ, Haimberger L, Healy SB, Hersbach H, Hólm EV, Isaksen I, Kållberg P, Köhler M, Matricardi M, McNally AP, Monge-Sanz BM, Morcrette JJ, Park BK, Peubey C, de Rosnay P, Tavolato C, Thépaut JN, Vitart F (2011). The ERA-Interim reanalysis: configuration and performance of the data assimilation system. *Q. J. Royal Met. Soc.* 137:553-597.
- Eklundh L (1998). Estimating relations between AVHRR NDVI and rainfall in East Africa at 10-day and monthly time scales. *Int. J. Remote Sens.* 19:563-568.
- Eklundh L, Sjöström M (2005). Analysing vegetation changes in the Sahel using sensor data from Landsat and NOAA. in: Proc Intl Sym Remote Sensing Environment, St. Petersburg FL.
- Hastenrath S (2000) Zonal circulations over the equatorial Indian Ocean. *J. Clim.* 13:2746-2756.
- Herrmann SM, Anyamba A, Tucker CJ (2005). Exploring relationship between rainfall and vegetation dynamics in the Sahel using coarse resolution satellite data. In: Proc Int. Symp. Remote Sens. Environ. June 20-24, St. Petersburg.
- Huete A, Didan K, Miura T, Rodriguez E, Gao X, Ferreira L (2002). Overview of the radiometric and biophysical performance of the MODIS vegetation indices, *Remote Sens. Environ.* 83:195-213.
- Jury MR, Huang B (2004) The Rossby wave as a key mechanism of Indian Ocean climate variability. *Deep Sea Res.* 51:2123-2136.
- Jury MR (2011). Climatic factors modulating Nile River flow, in Nile River Basin part IV, ed. AM Melesse, Springer, pp. 267-280.
- Jury MR (2013). Ethiopian highlands crop-climate prediction 1979-2009. *J. Appl. Meteorol. Climatol.* 52:1116-1126.
- Kanamitsu Ma, Wesley E, Jack W, Shi-Keng Y, Hnilo JJ, Fiorino M, Potter GL (2002) NCEP-DOE AMIP-II Reanalysis (R-2). *Bull. Amer. Meteor. Soc.* 83:1631-1643.
- Kawabata A, Ichi K, Yamaguchi Y (2001). Global monitoring of interannual changes in vegetation activities using NDVI and its relationships to temperature and precipitation. *Int. J. Remote Sens.* 22:1377-1382.
- Kennedy JJ, Rayner NA, Smith RO, Saunby M, Parker DE (2011). Reassessing biases and other uncertainties in sea-surface temperature observations since 1850 part 1: measurement and sampling errors. *J. Geophys. Res.* P. 116.
- Kogan FN (1998). A typical pattern of vegetation conditions in southern Africa during El Niño years detected from AVHRR data using three-channel numerical index. *Int. J. Remote Sens.* 19:3689-3695.
- Kug JS, An SI, Jin FF, Kang LS (2005). Preconditions for El Niño and La Niña onset and their relation to the Indian Ocean. *Geophys. Res. Lett.* 32:L05706.
- Kug JS, Li T, An SI, Kang LS, Luo JJ, Masson S, Yamagata T (2006). Role of the ENSO-Indian Ocean coupling in ENSO variability in a coupled GCM. *Geophys. Res. Lett.* 33:L09710.
- Lewis J E, Rowland J, Nadeau A (1998). Estimating maize production in Kenya using NDVI: some statistical considerations. *Int. J. Remote Sens.* 19:2609-2617.
- Li J, Lewis J, Rowland J, Tappan G, Tieszen LL (2004). Evaluation of land performance in Senegal using multi-temporal NDVI and rainfall series. *J. Arid Environ.* 59:463-480.
- Luo JJ, Zhang R, Behera SK, Masumoto Y, Jin FF, Lukas R, Yamagata T (2010). Interaction between El Niño and extreme Indian Ocean Dipole. *J. Clim.* 23:726-742.
- Maselli F, Romanelli S, Bottai L, Maracchi G (2000). Processing of GAC NDVI data for yield forecasting in the Sahelian region. *Int. J. Remote Sensing* 21: 3509-3523.
- Mennis J (2001) Exploring relationships between ENSO and vegetation vigour in the southeast USA using AVHRR data. *Int. J. Remote Sens.* 22:3077-3092.
- Myneni RB, Los SO, Tucker CJ (1996). Satellite-based identification of linked vegetation index and sea surface temperature anomaly areas from 1982-1990 for Africa, Australia, and South America. *Geophys. Res. Lett.* 23:729-732.
- Philippon N, Martiny N, Camberlin P, Hoffman MT, Gond V (2014). Timing and patterns of the ENSO Signal in Africa over the last 30 years: insights from Normalized Difference Vegetation Index data. *J. Climate* 27:2509-2532.

- Plisnier PD, Serneels S, Lambin EF (2000). Impact of ENSO on East African ecosystems: a multivariate analysis based on climate and remote sensing data. *Glob. Ecol. Biogeogr.* 9:481-497.
- Reed BC, Brown JF, VanDerZee D, Loveland TR, Merchant JW, Ohlen DO (1994). Measuring phenological variability from satellite imagery. *J. Vegetation Sci.* 5:703-714.
- Richard Y, Poccard I (1998). A statistical study of NDVI sensitivity to seasonal and interannual rainfall variations in Southern Africa. *Int. J. Remote Sens.* 19:2907-2920.
- Ropelewski CF, Halpert MS (1987). Global and regional scale precipitation patterns associated with El Niño/Southern Oscillation. *Mon Weather Rev.* 115:1606-1626.
- Rowell DP (2013). Simulating SST teleconnections to Africa: what is the state of the art? *J. Clim.* 26:5397-5418.
- Saji NH, Goswami BN, Vinayachandran PN, Yamagata T (1999) A dipole mode in the tropical Indian Ocean. *Nature* 401:360-363.
- Tucker CJ (1979) Red and photographic infrared linear combinations for monitoring vegetation. *Remote Sens. Environ.* 8:127-150.
- Tuckera CJ, Jorge EP, Molly EB, Daniel AS, Edwin WP, Robert M, Eric FV, El Saleousa N (2005). An extended AVHRR 8-km NDVI data set compatible with MODIS and SPOT vegetation NDVI data. *Int. J. Remote Sensing* 26:4485-5598.
- Vanacker V, Linderman M, Lupo F, Flasse S, Lambin E (2005). Impact of short-term rainfall fluctuation on interannual land cover change in sub-saharan Africa. *Glob. Ecol. Biogeogr.* 14:123-135.
- Verdin J, Funk C, Klaver R, Roberts D (1999) Exploring the correlation between Southern Africa NDVI and Pacific sea surface temperature: results for the 1998 maize growing season. *Int. J. Remote Sens.* 20:2117-2124.
- White MA, Thomton PE, Running SW (1997). A continental phenology model for monitoring vegetation responses to interannual climatic variability. *Glob. Biogeochem. Cycles* 11:217-234.
- White WB, Tourre YM (2003). Global SST/SLP waves during the 20th century. *Geophys. Res. Lett.* 30:53-57.
- White WB, Tourre YM (2007). A delayed action oscillator shared by the ENSO and QDO in the Indian Ocean. *J. Oceanogr.* 63:223-241.
- Young SS, Harris R (2005). Changing patterns of global-scale vegetation photosynthesis, 1982–1999. *Int. J. Remote Sens.* 26:4537-4563.
- Zhang X, Friedl MA, Schaaf CB, Strahler AH (2005). Monitoring the response of vegetation phenology to precipitation in Africa by coupling MODIS and TRMM instruments. *J. Geophys. Res.* P. 110.